RSC Advances

PAPER

View Article Online
View Journal | View Issue

Cite this: *RSC Adv.*, 2014, **4**, 784

Mesoporous silicas templated by symmetrical multiblock copolymers through evaporation-induced self-assembly

Wei-Cheng Chu, Shih-Fan Chiang, Jheng-Guang Li and Shiao-Wei Kuo*

Received 25th September 2013
Accepted 12th November 2013

DOI: 10.1039/c3ra45348k

www.rsc.org/advances

In this study, we synthesized long-range-ordered mesoporous silicas through evaporation-induced self-assembly (EISA), templated by the ABA-type triblock copolymer PEO-PPO-PEO (F127), and found that the morphologies of the mesostructures could be controlled from a hexagonal cylinder structure to a body-centered cubic (bcc) structure by varying the amount of added tetraethyl orthosilicate (TEOS). In addition, we synthesized the multiblock ABCBA-type copolymer PCL-PEO-PPO-PEO-PCL (PCL-F127-PCL) through ring-opening polymerization (using F127 as the macro-initiator) and then examined the effect of its PCL segments on the morphology of the resulting mesoporous silica. We employed small-angle X-ray scattering (SAXS), transmission electron microscopy (TEM), and N_2 adsorption/desorption isotherms to investigate the mesophase transformations of these mesoporous nanostructures containing various TEOS contents. Upon increasing the molecular weight of the PCL segments, the *d*-spacing decreased initially, but then increased thereafter. The PCL-F127-PCL multiblock copolymer assembled into an "m"-shaped structure, with the hydrophilic PEO segments folded outside and the hydrophobic PCL and PPO segments aggregated inside. In addition to the relatively strong interactions with the PCL segments, the hydrophilic PPO segments also interacted relatively strongly with the silica matrix, such that some of the PPO segments could enter within it. Using this approach with ABA-type triblock and ABCBA-type multiblock copolymers as templates, we can prepare highly ordered mesoporous silicas having narrow pore size distributions and various mesoporous structures.

Introduction

Mesoporous materials having controlled pore sizes are attractive to both the academic and industrial communities because of their applications in various fields, including filtering, separating, sensing, catalysis, and controlled drug release.[1–5] Ordered mesoporous materials have attracted much attention since Mobil scientists first reported the synthesis of mesoporous silicas using the cationic surfactant cetyltrimethylammonium bromide [$C_{16}H_{33}N(CH_3)_3Br$, CTAB] as the template, obtaining highly ordered mesoporous molecular sieves (M41S) under hydrothermal and basic conditions.[6,7] Following that initial report, the Stucky group synthesized a further series of mesoporous silicas (*e.g.*, SBA-n) when using poly(ethylene oxide-*b*-propylene oxide-*b*-ethylene oxide) (PEO-PPO-PEO) triblock copolymers as templates in a water-soluble system.[8,9] As a result, several commercial strategies have been developed based on PEO-PPO-PEO triblock copolymers as templates to obtain many highly ordered large-pore mesoporous silicas.[8–30] Nevertheless, PEO-PPO-PEO triblock copolymers are seldom capable of directly templating ordered mesoporous silicas with larger pore sizes because of limitations related to their composition and molecular weight. Although those developed approaches toward mesoporous silicas have been restricted to water-soluble systems, a majority of amphiphilic block copolymers are only sparingly soluble in aqueous solutions.

Accordingly, evaporation-induced self-assembly (EISA) has been used to prepare mesoporous silicas templated by high-molecular-weight amphiphilic block copolymers.[31–41] The EISA strategy can also be used broadly for the preparation of mesoporous organic materials, mesoporous polymer resins,[31,42–49] and mesoporous carbons.[32,50–56] In other words, EISA provides an approach toward the formation of ordered mesoporous nanostructures[57–59] when combined with unusual AB diblock copolymers[31,32,37] or ABC triblock terpolymers[35] as templates. Many studies of mesoporous materials have been performed because of their potential applications in catalysis,[60] adsorption,[61] and drug delivery.[3] Meanwhile, many research groups are interested in the factors influencing the transformations of the self-assembled morphologies[62–64] and the mechanisms of fabricating these ordered mesoporous materials.[65–69]

In this study, we used PEO-PPO-PEO (F127), an ABA-type triblock polymer, as a template to prepare order mesoporous

Department of Materials and Optoelectronic Science, Center for Nanoscience and Nanotechnology, National Sun Yat-Sen University, Kaohsiung, 804, Taiwan. E-mail: kuosw@faculty.nsysu.edu.tw

silicas through an EISA strategy. We found that increasing the ratio of tetraethyl orthosilicate (TEOS) to F127 in the mixtures, the morphology of the mesophase changed from a hexagonal cylinder structure to a body-centered cubic (bcc) structure. To the best of our knowledge, no previous reports have described the use of a single template as a structure-directing agent in the syntheses of two different types of long-range-ordered mesostructured silicas, merely by changing the relative amount of TEOS. Similarly, in previous studies,[31,59] we used a double-crystalline amphiphilic block copolymer, poly(ethylene oxide-*b*-ε-caprolactone) (PEO-*b*-PCL), of a single high molecular weight and possessing long hydrophobic segments, as the template for the preparation of large mesoporous silica structures, where the pore dimensions were related primarily to the molecular weights of the hydrophobic segments. The morphologies and pore sizes of the mesoporous silicas were dependent on the molecular weight and hydrophilic/hydrophobic segment ratio of the templates, and observed transformations of the mesophase occurred upon varying the TEOS-to-template weight fraction. Accordingly, in this study we also used ring-opening polymerization to synthesize a series of PCL-F127-PCL ABCBA-type multiblock copolymers ($CL_{12}EO_{106}PO_{70}EO_{106}CL_{12}$ and $CL_{45}EO_{106}PO_{70}EO_{106}CL_{45}$) that we then employed to regulate the morphologies and pore sizes of mesoporous silicas in response to the molecular weight of the PCL segments. Here, we used small-angle X-ray scattering (SAXS), transmission electron microscopy (TEM), and N_2 adsorption/desorption isotherms to characterize the changes in the structures and sizes of the mesoporous materials during the EISA processes.

Experimental

Materials

All chemicals were used as received without purification. TEOS (99%) and hydrochloric acid were obtained from SHOWA. Ethanol (95%) and tetrahydrofuran (THF, >99%) were purchased from ECHO. De-ionized water was used in all experiments. The triblock copolymer poly(ethylene oxide-*b*-propylene oxide-*b*-ethylene oxide), Pluronic F127 ($EO_{106}PO_{70}EO_{106}$), with a molecular weight of 12 600 was obtained from Aldrich and dried through azeotropic distillation with dry toluene. ε-Caprolactone (ε-CL, Acros) was purified by vacuum distillation over CaH_2. The distillation fraction collected at 96–98 °C (5 mm-Hg) was used in all polymerizations. Stannous(II) octoate [$Sn(Oct)_2$, Sigma] was used as received. Methylene chloride was dried over CaH_2 prior to use. Multiblock copolymers were readily prepared through ring-opening polymerization of ε-CL and Pluronic F127 in the presence of $Sn(Oct)_2$ as the catalyst.[70]

PCL-PEO-PPO-PEO-PCL multiblock copolymers (PCL-F127-PCL)

A desired volume of ε-CL monomer was placed in a silanized flask containing a pre-weighed amount of Pluronic F127 under a N_2 atmosphere. $Sn(Oct)_2$ (1 drop) was added and then the flask was connected to a vacuum line, evacuated, sealed off, and heated at 130 °C. After 24 h, the resulting block copolymers were dissolved in CH_2Cl_2 and precipitated in excess of cold *n*-hexane. The polymers were dried at 40 °C under vacuum. The characterization data of the multiblock copolymers tested in this study are summarized in Table 1. Yield: 77%; ^{1}H NMR (500 MHz, $CDCl_3$, Fig. 1): δ 4.10 (t, OCH_2, PCL), 3.65 (s, CH_2CH_2O, PEO), 3.55 [s, $CH_2CH(CH_3)$, PPO], 3.55 [s, $CH(CH_3)O$, PPO], 3.35 (s, OCH_3, PEO), 2.30 (t, 2H, PCL), 1.63 (m, 4H, PCL), 1.38 (m, 2H, PCL), 1.11 (s, CH_3, PPO).

Mesoporous silica

Mesoporous silicas were prepared through an EISA strategy in THF, using a copolymer ($EO_{106}PO_{70}$ EO_{106}, $CL_{12}EO_{106}PO_{70}EO_{106}CL_{12}$, $CL_{45}EO_{106}PO_{70}EO_{106}CL_{45}$) as the template and TEOS as the silica precursor (Scheme 1). Various TEOS-to-F127 or TEOS to PCL-*b*-F127-*b*-PCL ratios (Table 2) were used at a constant $HCl_{(aq.)}$ concentration [0.1 g of 0.1 M $HCl_{(aq.)}$ in 5 g of THF]; TEOS was added into a THF (5 g) solution of the block copolymer (2.0 wt%, containing 0.10 g of copolymer), with stirring, which was continued for 30 min to form a homogeneous solution. The sample was poured into a Petri dish and the THF was evaporated at room temperature for 48 h. The transparent film was collected and ground into a powder, which was then transferred to a PFA bottle containing 1.0 M HCl (30 mL) and treated hydrothermally at 100 °C for 3 days. The product was washed with water and EtOH, dried at room temperature, and calcined in air at 600 °C for 6 h to produce a white

Table 1 Characterization of the PCL-*b*-F127-*b*-PCL multiblock copolymers tested in this study

Multiblock copolymer PCL-*b*-F127-*b*-PCL	M_n [a]	M_n [b]	M_W/M_n [b]
$CL_{12}EO_{106}PO_{70}EO_{106}CL_{12}$ (CFC1)	15 336	27 000	1.15
$CL_{45}EO_{106}PO_{70}EO_{106}CL_{45}$ (CFC2)	22 860	40 000	1.18

[a] Obtained by ^{1}H NMR spectra. [b] Obtained by GPC trace with DMF eluent of 0.6 ml min^{-1} and PS-standard calibration.

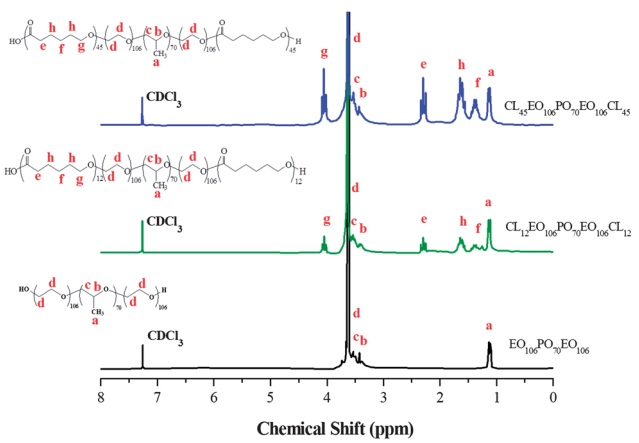

Fig. 1 ^{1}H NMR spectra ($CDCl_3$) of the block copolymers $EO_{106}PO_{70}EO_{106}$ (F127), $CL_{12}EO_{106}PO_{70}EO_{106}CL_{12}$ (CFC1), and $CL_{45}EO_{106}PO_{70}EO_{106}CL_{45}$ (CFC2).

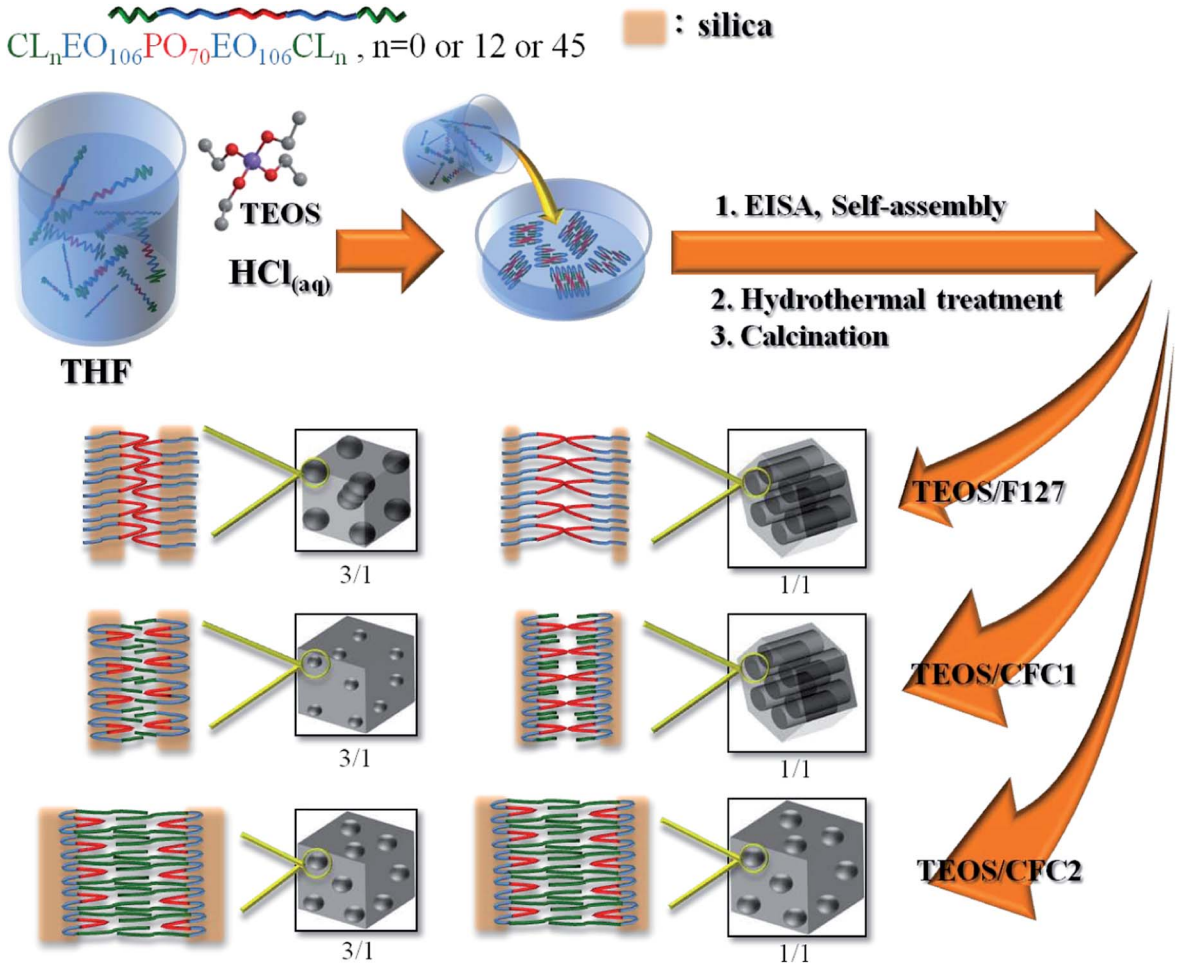

Scheme 1 Preparation of mesoporous silicas under various conditions.

Table 2 Textural properties of mesoporous silicas templated by various block copolymers

Samples	d (nm)[a]	Pore size (nm)	Wall thickness (nm)	S_{BET} (m^2 g^{-1})[b]	Pore volume (cm^3 g^{-1})	Micropore volume (cm^3 g^{-1})	TEOS/template (weight fraction)
C0T1	11.9	11.1	2.6	773	0.99	0.03	TEOS/F127 = 1/1
C0T2	11.9	6.6	7.9	830	0.91	0.04	TEOS/F127 = 2/1
C0T3	10.8	4.8	8.5	831	0.71	0.08	TEOS/F127 = 3/1
C0T4	10.5	4.0	8.8	806	0.60	0.10	TEOS/F127 = 4/1
C0T5	10.3	3.4	9.2	719	0.46	0.11	TEOS/F127 = 5/1
C0T6	10.1	2.9	9.5	704	0.42	0.11	TEOS/F127 = 6/1
C1T1	10	7.5	4.0	855	1.12	0.02	TEOS/CFC1 = 1/1
C1T2	10.8	6.6	6.7	846	1.03	0.07	TEOS/CFC1 = 2/1
C1T3	10.0	4.7	7.5	641	0.61	0.08	TEOS/CFC1 = 3/1
C1T4	10.0	4.7	7.5	530	0.46	0.08	TEOS/CFC1 = 4/1
C1T5	9.5	4.7	7.0	547	0.50	0.07	TEOS/CFC1 = 5/1
C1T6	9.2	3.4	7.9	610	0.43	0.11	TEOS/CFC1 = 6/1
C2T1	16.1	11.7	8.0	668	1.04	0.07	TEOS/CFC2 = 1/1
C2T2	17	11.4	9.4	703	0.91	0.07	TEOS/CFC2 = 2/1
C2T3	18	11.4	10.7	749	0.83	0.13	TEOS/CFC2 = 3/1
C2T4	18.5	11.5	11.2	613	0.63	0.10	TEOS/CFC2 = 4/1
C2T5	19.0	10.0	13.3	554	0.52	0.10	TEOS/CFC2 = 5/1
C2T6	20.3	10.1	14.8	377	0.36	0.10	TEOS/CFC2 = 6/1

[a] The d-spacing values were calculated from the first SAXS peak by the formula $d = 2\pi/q^*$. [b] S_{BET} and S_M are the total BET surface area and micropore surface area calculated from the t-plots, respectively.

mesoporous silica. Calcination processes were conducted in a furnace operated at a heating rate of 1 °C min^{-1}.

Characterization

SAXS data were recorded using a NANOSTAR U small-angle X-ray scattering system (Bruker AXS, Karlsruhe, Germany) and Cu Kα radiation (30 W, 50 kV, 600 μA). The *d*-spacings were calculated using the formula, $d = 2\pi/q$, where q is the scattering vector. TEM images were recorded using a JEOL 3010 microscope operated at 200 kV; the samples were suspended in EtOH and supported onto a holey carbon film on a Cu grid. Nitrogen adsorption/desorption isotherms were measured at 77 K using an ASAP 2020 analyzer. Prior to measurement, the samples were degassed under vacuum at 200 °C for at least 6 h. The Brunauer–Emmett–Teller (BET) method was employed to calculate the specific surface areas and pore volumes; pore size distributions were derived from the adsorption branches of the isotherms.

Results and discussion

Synthesis of mesoporous silicas at various TEOS/F127 ratios

We prepared the mesoporous silica samples C0T1–C0T6 by employing the triblock copolymer F127 as the template at TEOS-to-F127 ratios of 1 : 1, 2 : 1, 3 : 1, 4 : 1, 5 : 1, and 6 : 1, respectively. Fig. 2(a) displays the SAXS patterns of samples of C0T1–C0T6; the *d*-spacings of the mesoporous silicas decreased from 11.9 nm (C0T1) to 10.1 nm (C0T6) upon increasing the weight ratio of TEOS. Furthermore, the SAXS reflection sets also changed from hexagonal cylindrical features [(100), (110), (200)] for C0T1 (TEOS/F127 = 1 : 1) to cubic characteristics [(110), (211), (220)] for C0T3 (TEOS/F127 = 3 : 1) upon varying the content of TEOS. TEM images [Fig. 2(b)–(g)] confirmed that the morphologies of the mesoporous silicas varied from a hexagonal cylindrical structure (along [001]), to a bcc structure (along [100]), and finally to a disordered micelle structure.

Thus, we could use the EISA method to synthesize new mesoporous silicas exhibiting a morphological transformation from a hexagonal cylinder structure to a bcc structure when applying the F127 triblock copolymer, which had a large volume fraction of its hydrophilic EO block segment, as the template at TEOS/F127 ratios of 1 : 1 and 3 : 1. The SAXS pattern [Fig. 3(a)] of the bcc-type mesoporous silica C0T3 exhibited a strong reflection having a *d*-spacing of 10.8 nm, one strong reflection at a value of q of 0.99 nm^{-1}, and one weaker reflection at a value of q of 1.13 nm^{-1}; this SAXS pattern could be indexed as having (110), (211), and (220) reflections, corresponding to a cubic structure ($Im\bar{3}m$ space group). In addition, we also confirmed the structural ordering and cubic symmetry of this material through TEM analyses. Fig. 3(b)–(d) display TEM images of the bcc-type mesoporous phenolic resin with different orientations ([100], [110], and [111] planes, respectively). Notably, these conditions enabled the facile and highly reproducible preparation of a large-cage three-dimensional (3D) cubic mesoporous

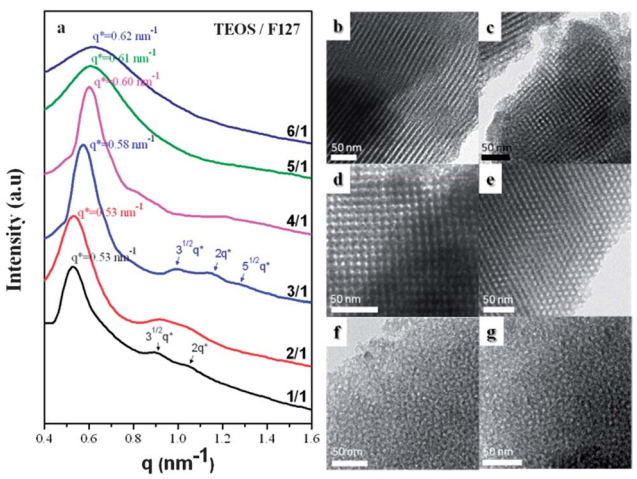

Fig. 2 (a) SAXS patterns and (b–g) TEM images of mesoporous silicas templated at TEOS-to-F127 weight ratios of (b) 1 : 1, (c) 2 : 1, (d) 3 : 1, (e) 4 : 1, (f) 5 : 1, and (g) 6 : 1.

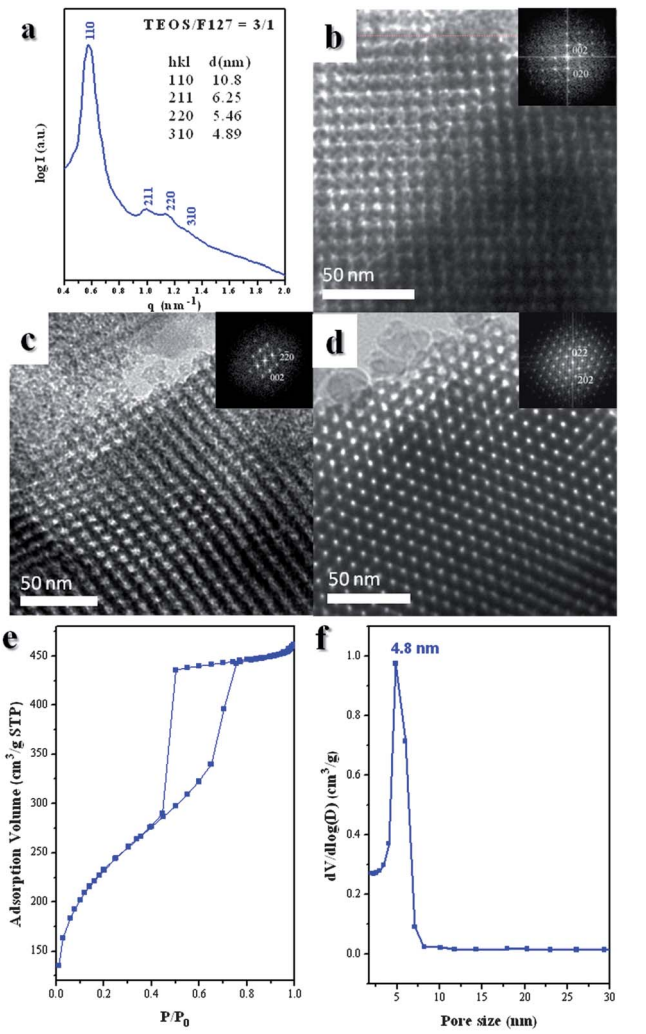

Fig. 3 (a) SAXS pattern, (b–d) TEM images viewed from (b) [100], (c) [110], and (d) [111] (insets: corresponding FFT), (e) N_2 adsorption/desorption isotherm, and (f) pore size distribution curve of the bcc mesoporous silica templated by F127 at a TEOS-to-F127 ratio of 3 : 1.

phenolic resin having $Im\bar{3}m$ symmetry. We obtained further information regarding the textural properties of the materials from N_2 adsorption/desorption isotherms measured at 77 K. Fig. 3(e) presents the N_2 sorption isotherms of the cubic mesoporous silica sample. The sample displays individual type-IV isotherms, exhibiting the apparent H_2 hysteresis loop characteristic of a cage-like mesoporous material. A sharp capillary condensation step appeared for this sample, suggesting uniform pore dimensions and high-quality ordering of the materials, in agreement with the TEM and SAXS data. Pore size distribution analysis revealed [Fig. 3(f)] a well-ordered cubic structure having pores with an average diameter of approximately 4.8 nm.

Fig. 4(a) summarizes the N_2 sorption isotherms of the mesoporous silica samples obtained at various TEOS/F127 ratios; each appeared as a representative type-IV curve. Table 2 summarizes the BET surface areas, pore volumes, and BJH pore sizes of these mesoporous silica materials. The sample C0T1 (TEOS/F127 = 1 : 1) exhibited a typical H_1-like hysteresis loop at values of P/P_0 from 0.4 to 0.85, suggesting a cylindrical mesoporous structure. Increasing the TEOS content resulted in all of the samples exhibiting typical H_2-like hysteresis loops, characteristic of spherical mesopores. Fig. 4(b) displays the pore size distribution curves. The average pore size of sample C0T1 was 11.1 nm (determined using the Harkins–Jura model); the other samples featured average pore sizes [determined using the Broekhoff–de Boer (BdB) model] that decreased from 6.6 to 2 nm upon increasing the TEOS content. In addition, the wall thickness (Table 2) increased upon increasing the TEOS content, inversing the trend for the average pore size. Thus, the TEOS content influenced the mesoporous structure, average pore size, and wall thickness because it increased the hydrophilic volume ratio in conjunction with the PPO segments. Increasing the TEOS content caused the mesoporous structures to transform from hexagonal cylindrical structures *via* bcc structures to disorder sphere structures. This paper reports the first example of the preparation of two kinds of long-range-ordered mesoporous silica structures—a hexagonal cylinder structure (TEOS/F127 = 1 : 1) and a bcc structure (TEOS/F127 = 1 : 3)—from a single template (F127), merely by changing the TEOS content.

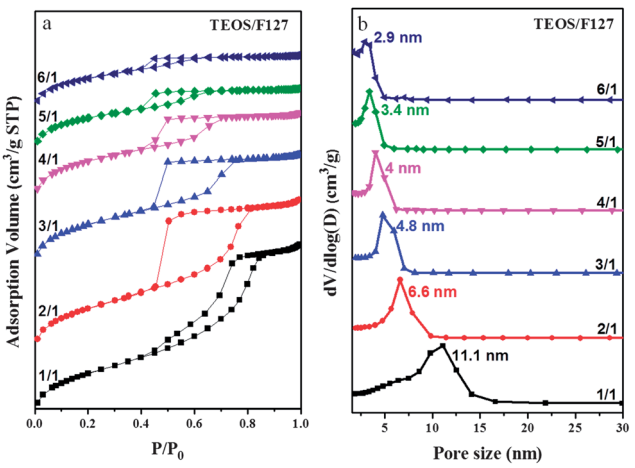

Fig. 4 (a) Nitrogen adsorption/desorption isotherms and (b) pore size distribution curves of mesoporous silicas templated at TEOS/F127 weight ratios of 1 : 1, 2 : 1, 3 : 1, 4 : 1, 5 : 1, and 6 : 1.

Mesoporous silicas prepared using PCL-F127-PCL ABCBA-type multiblock copolymer

To study the effect of the hydrophobic PCL segments in ABCBA-type multiblock copolymers PCL-F127-PCL during the EISA process used for the synthesis of mesoporous silicas, we prepared two PCL-F127-PCL multiblock copolymers (Table 1) featuring different PCL contents: $CL_{12}EO_{106}PO_{70}EO_{106}CL_{12}$ (CFC1; M_n = 15 336) and $CL_{45}EO_{106}PO_{70}EO_{106}CL_{45}$ (CFC2; M_n = 22 860). Fig. 5 displays SAXS patterns and TEM images of mesoporous silicas templated by CFC1 at various TEOS-to-CFC1 weight ratios. The mesoporous silica possessed a hexagonal cylinder morphology at a relatively low TEOS-to-CFC1 ratio of 1 : 1, as revealed in the both the SAXS pattern [approximate relative values of q of $q^* = 0.63$ nm^{-1}, $3^{1/2}$ q^*, and $4^{1/2}$ q^* in Fig. 5(a)] and TEM image [see side view of the cylinder structure in Fig. 5(b)]. Increasing the ratio of TEOS to CFC1 from 1 : 1 to 6 : 1 (from sample C1T1 to sample C1T6), a change in morphology from cylinders to disorder micelles was evident in the SAXS pattern in Fig. 5(a) and the TEM images in Fig. 5(b)–(g).

Fig. 6 presents N_2 sorption isotherms of the mesoporous silica samples prepared at the various TEOS-to-CFC1 weight ratios; they appear as representative type-IV curves. The sample C1T1 provided a capillary condensation step in the relative pressure range from 0.4 to 0.8, thereby exhibiting a typical H_1-like hysteresis loop, characteristic of cylindrical mesopores, indicating a narrow pore size distribution centered at 7.5 nm [Fig. 6(b)]. The sample C1T2 provided similar type-IV isotherms with an H_2-type hysteresis loop, but a sluggish desorption capillary condensation occurred at a relative pressure ranging from 0.8 to 0.7 and a sharp desorption capillary condensation occurred at a relative pressure ranging from 0.7 to 0.4, implying the presence of two different types of mesopores. This structure was confirmed in the TEM image in Fig. 5(c), which reveals both cylindrical mesopores and disordered spheres. The other mesoporous silica samples exhibited typical H_2-like hysteresis loops with a sharp capillary condensation step in the relative pressure range from 0.4 to 0.7, characteristic of spherical mesopores [Fig. 6(a)]. The pore size distributions, derived from the adsorption branches, narrowed significantly upon increasing the TEOS content (Table 2). Accordingly, we conclude that the PCL and PPO segments behaved as the hydrophobic segments that provided the mesopores of the mesostructures and induced the phase transformation from hexagonal cylindrical structures to disorder spherical structures. We also observed that the wall thickness (Table 2) of the mesoporous silicas increased from 4 nm (for C1T1, determined from the cylinder wall-thickness equation) to 7.9 nm (for C1T6, determined using the sphere wall-thickness equation) upon increasing the weight ratio of TEOS. Notably, some of the PPO segments presumably entered the silica matrix because the PPO segments were not sufficiently

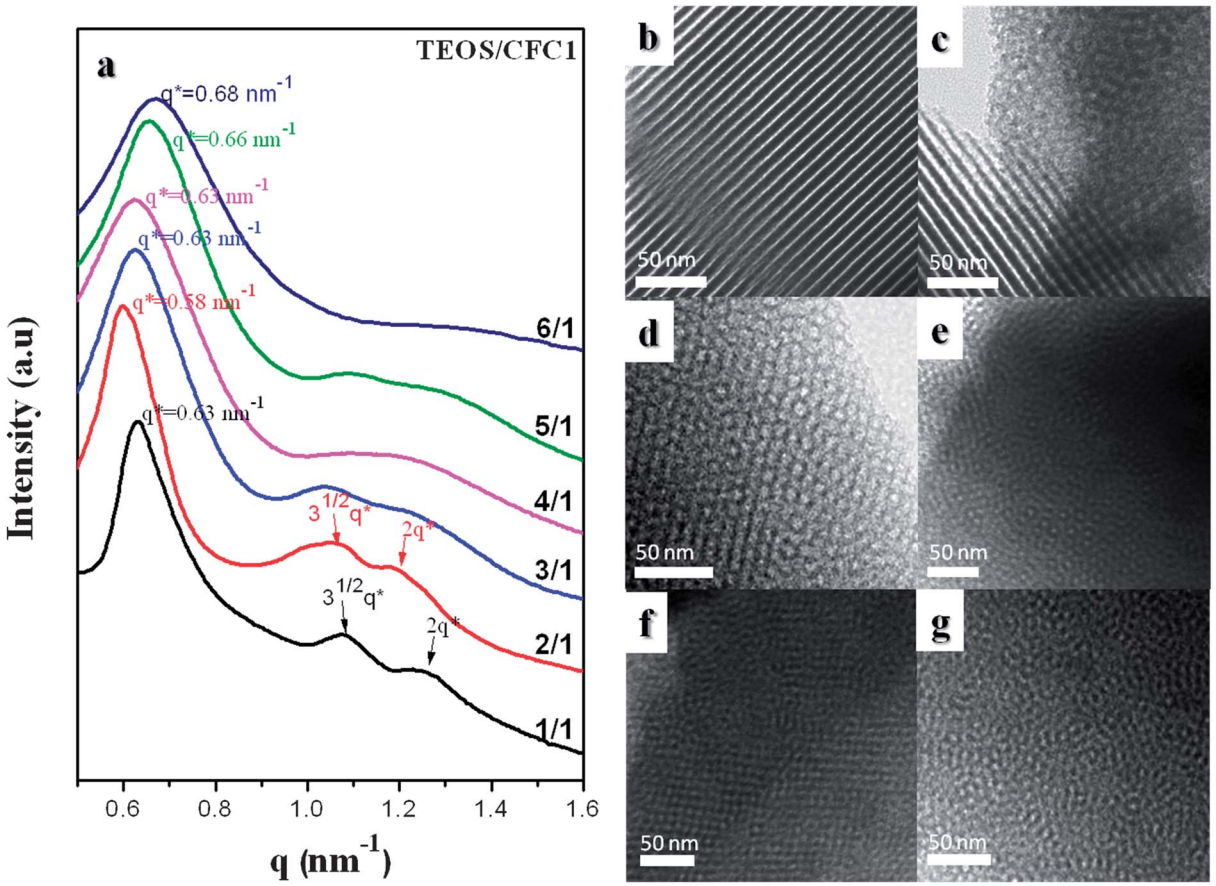

Fig. 5 (a) SAXS patterns and (b–g) TEM images of mesoporous silicas templated by TEOS/CFC1 at weight ratios of (b) 1 : 1, (c) 2 : 1, (d) 3 : 1, (e) 4 : 1, (f) 5 : 1, and (g) 6 : 1.

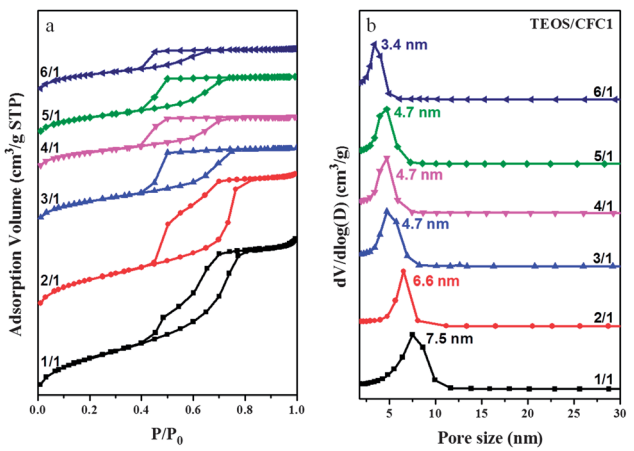

Fig. 6 (a) Nitrogen adsorption/desorption isotherms and (b) pore size distribution curves of mesoporous silicas templated by TEOS/CFC1 at weight ratios of 1 : 1, 2 : 1, 3 : 1, 4 : 1, 5 : 1, and 6 : 1.

hydrophobic; its interaction with the silica matrix became relatively weaker upon increasing the TEOS content.

Fig. 7 displays SAXS patterns and TEM images of the mesoporous silica samples obtained from the systems templated by the ABCBA-type block copolymer $CL_{45}EO_{106}PO_{70}EO_{106}CL_{45}$ (CFC2; M_n = 22 860) at various TEOS-to-CFC2 weight ratios. These mesoporous silicas all featured long-range-disordered spherical mesostructures when prepared at TEOS-to-CFC2 ratios from 1 : 1 to 6 : 1, as confirmed by both the SAXS patterns

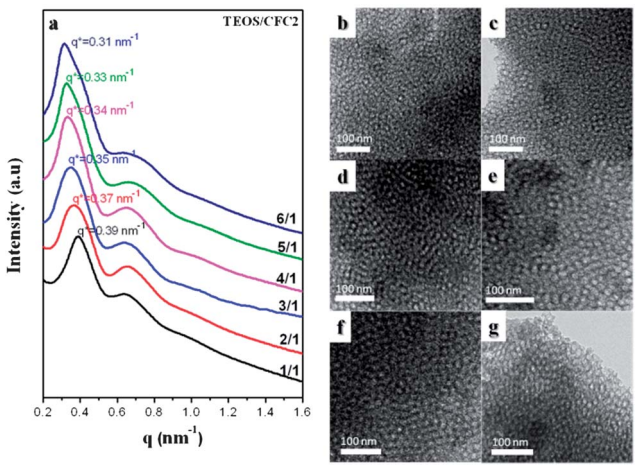

Fig. 7 (a) SAXS patterns and (b–g) TEM images of mesoporous silicas templated by TEOS/CFC2 at weight ratios of (b) 1 : 1, (c) 2 : 1, (d) 3 : 1, (e) 4 : 1, (f) 5 : 1, and (g) 6 : 1.

[two distinct peaks in Fig. 7(a)] and TEM images [Fig. 7(b)–(g)]. The *d*-spacings of the spherical mesoporous silicas increased upon increasing the TEOS content, from 16.1 nm for C2T1 to 20.3 nm for C2T6. The N_2 sorption isotherms of the mesoporous silicas templated by CFC2 exhibit (Fig. 8) typical type-IV curves with a large H_2-type hysteresis loop, suggesting caged mesostructures. The sharp capillary condensation in the relative pressure range between 0.45 and 0.9 suggests a narrow pore size distribution centered at 10–11 nm [Fig. 8(b)]. We also found that the wall thicknesses of the mesoporous silicas (Table 2, sphere wall-thickness equation) increased from 8.0 nm for C2T1 to 14.0 nm for C2T6 upon increasing the TEOS content. On the basis of these results, we speculate that the PCL segments were mainly responsible for the mesopores of the disordered spherical mesostructures, because PCL segments are more hydrophobic than PPO segments. Here, in the case of CFC2 block copolymer, average pore size remains same (Fig. 8(b)), is different with F127 and CFC1 that the average pore size was decreased upon increasing the TEOS content. We found that the wall thickness was increasing upon increasing the TEOS content in all cases. The pore volume and pore size were mainly composed of the hydrophobic segments of PPO and PCL. In case of F127 block copolymer, the PPO segments have a weak interaction within silica matrix and thus partial PPO segments should enter silica matrix, and therefore average pore size was decreased upon increasing the TEOS content. Similarly, the trend could be observed in CFC1 block copolymer, where the molecular structure assemblies like "*m*" shape, the PEO segments fold outside, and the PCL segments and PPO segment aggregate inside since the molecular weight of PPO was larger than PCL, the pore volume and pore size were mainly composed of both them. However, when the molecular weight of PCL was greater than PPO in CFC2, therefore the pore volume and pore size were mainly composed of PCL segments. The influence of PPO segments on the pore volume and pore size were feeble that resulting in average pore size remains same upon increasing the TEOS content.

Effect of hydrophobic PCL segments in symmetrical multiblock copolymer of mesoporous silicas

In a previous study of mesoporous silica structures templated by PEO-*b*-PCL, we found that the morphology changed and the pore size increased upon increasing the content of PCL segments.[59] In this present study, we were curious to discern whether the phenomena would also occur when using different templates. Fig. 9 presents SAXS patterns and TEM images of the mesoporous silicas prepared from different templates at a constant TEOS-to-template ratio of 1 : 1. The SAXS profiles of samples C0T1 and C1T1 [Fig. 9(a)] feature organized peaks having a peak ratio of $1 : 3^{1/2} : 4^{1/2}$. Both SAXS patterns reveal clear hexagonal cylindrical packing, which was confirmed by the TEM images [Fig. 9(b)–(e)] viewed from the [10] direction {side views of cylinder structures: Fig. 9(b) (C0T1) and Fig. 9(d) (C1T1)} and the [001] direction {top views of cylinder structures: Fig. 9(c) (C0T1) and Fig. 9(e) (C1T1)}. Sample C2T1 provided different well-resolved SAXS peaks [Fig. 9(a)] at a value of q^* of 0.39 nm^{-1} (16.1 nm) and its TEM images [Fig. 9(f) and (g)] revealed a disordered micelle structure. Samples C0T1 and C1T1 both exhibited type-IV curves with typical H_1-like hysteresis loops at values of P/P_0 ranging from 0.4 to 0.85 and from 0.4 to 0.8, respectively, characteristic of cylindrical mesopores [Fig. 10(a)]. Increasing the PCL segments of molecular weight resulted in the sample C2T1 exhibiting a typical H_2-like hysteresis loop at values of P/P_0 ranging from 0.43 to 0.9, suggesting a common spherical mesoporous structure [Fig. 10(a)]. Table 3 summarizes the BET surface areas, pore volumes, and BJH pore sizes of these mesoporous silica materials. The mean pore sizes [Fig. 10(b)] in samples C0T1 and C1T1 (determined using the Harkins–Jura model) and in sample C2T1 (determined using the BdB model, measured from the adsorption branches) were 11.1, 7.5, and 11.7, respectively. Interestingly, when templating using the ABCBA symmetrical multiblock copolymer featuring the low-molecular-weight PCL segment, the resulting sample C1T1 featured smaller pores and a shorter *d*-spacing than those of sample C0T1. In a previous study, Jung *et al.* found[71] that the self-assembled structure formed from a F127 triblock copolymer varied from a micelle to vesicle

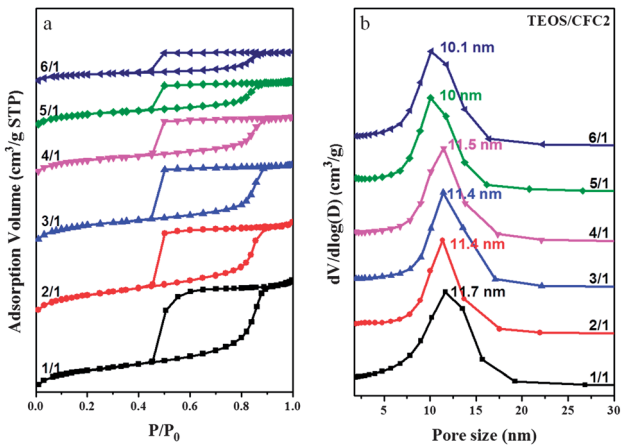

Fig. 8 (a) Nitrogen adsorption/desorption isotherms and (b) pore size distribution curves of mesoporous silicas templated by TEOS/CFC2 at weight ratios of 1 : 1, 2 : 1, 3 : 1, 4 : 1, 5 : 1, and 6 : 1.

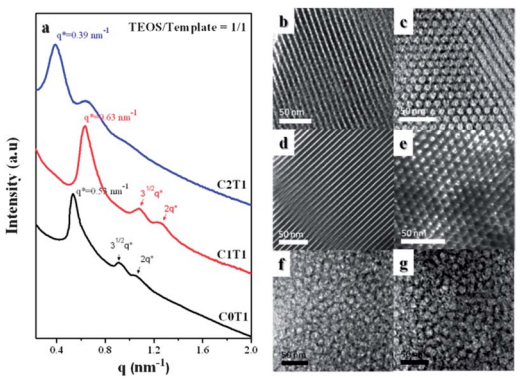

Fig. 9 (a) SAXS patterns and (b–g) TEM images of mesoporous silicas templated by (b and c) F127, (d and e) CFC1, and (f and g) CFC2 at TEOS-to-template weight ratios of 1 : 1.

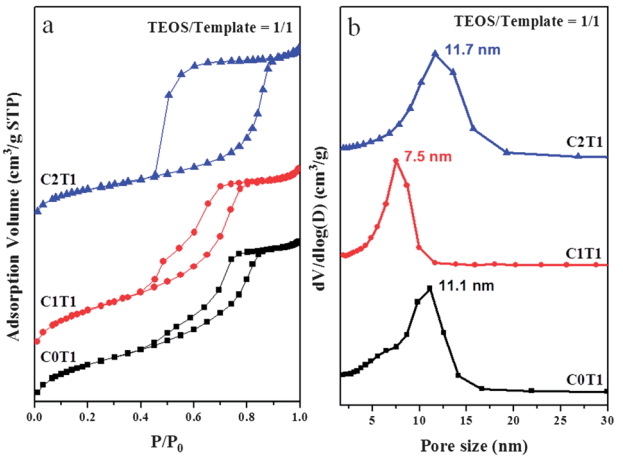

Fig. 10 (a) Nitrogen adsorption/desorption isotherms and (b) pore size distribution curves of mesoporous silicas templated by F127, CFC1, and CFC2 at TEOS-to-template weight ratios of 1 : 1.

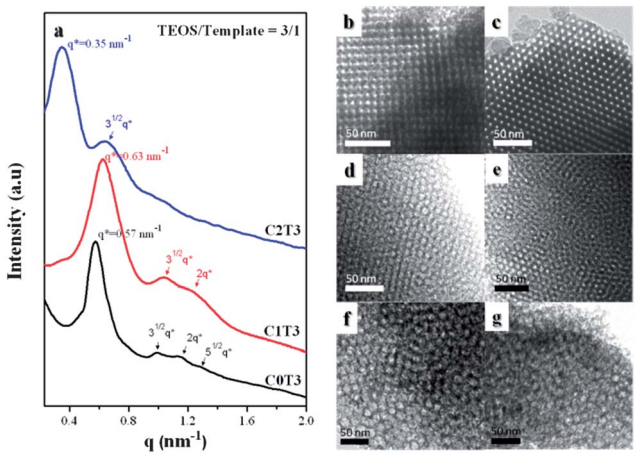

Fig. 11 (a) SAXS patterns and (b–g) TEM images of mesoporous silicas templated by (b and c) F127, (d and e) CFC1, and (f and g) CFC2 at TEOS-to-template weight ratios of 3 : 1.

structure when the PCL-F127-PCL multiblock copolymer featured PCL segments of relatively low molecular weight, but formed bridged micelle structures when the PCL segments were of relatively high molecular weight. Upon increasing the molecular weight of the PCL segments, the average size of the micelles decreased initially, but increased thereafter.[72] We observed similar behavior in this present study: upon increasing the molecular weight of the PCL segments, the *d*-spacing decreased initially, but increased thereafter. Therefore, we surmise that the molecules assembled into a structure having an "m" shape, with the hydrophilic PEO segments of PCL-F127-PCL folded on the outside and the hydrophobic PCL and PPO segment aggregating inside. In addition to a relatively strong hydrophilic interactions with the PCL segments, the PPO segments interacted weakly with the silica matrix and, therefore, partially entered within it.

Fig. 11 presents SAXS patterns and TEM images of the mesoporous silicas prepared using different templates at a constant TEOS-to-template ratio of 3 : 1. The SAXS profile of sample C0T3 exhibited [Fig. 11(a)] organized peaks (q^* = 0.57 nm^{-1}; d = 10.8 nm) having a peak ratio of $1 : 3^{1/2} : 4^{1/2} : 5^{1/2}$. The SAXS pattern and TEM images [Fig. 11(b) and (c)] suggested a clear bcc structure. Samples C1T3 and C2T3 provided different, well-resolved SAXS peaks [Fig. 11(a)] at values of q^* of 0.63 nm^{-1} (d = 10 nm) and 0.35 nm^{-1} (d = 18 nm), respectively. TEM images revealed that the morphology transformed from a bcc structure to part rule micelles [sample C1T3, Fig. 11(d) and (e)] and, finally, to a disordered micelle structure [sample C2T3, Fig. 11(f) and (g)]. In Fig. 12(a), the N_2 sorption isotherms of these mesoporous silica samples were all representative type-IV curves; they all provided H_2-like hysteresis loops at values of P/P_0 ranging from 0.45 to 0.75 for C0T3, from 0.40 to 0.75 for C1T3, and from 0.45 to 0.85 for C2T3, indicative of spherical mesoporous structures. Fig. 12(b) displays the pore size distributions, measured from the adsorption branches, based on the BdB model; upon increasing the molecular weight of the PCL segments, the average pore size decreased initially, but increased thereafter. Table 3 summarizes the *d*-spacings, BJH pore sizes, wall thicknesses (using the equation for the wall thickness of bcc structures), BET surface areas, pore volumes, and micropore volumes of the various

Table 3 Textural properties of mesoporous silicas templated by F127, CFC1, and CFC2 at TEOS/template = 1/1 and 3/1 weight ratios

Sample	d (nm)	Pore size (nm)	Wall thickness (nm)	S_{BET} ($m^2\ g^{-1}$)	Pore volume ($cm^3\ g^{-1}$)	Micropore volume ($cm^3\ g^{-1}$)
C0T1	11.9	11.1	2.6	773	0.99	0.025
C1T1	10.0	7.5	4.0	855	1.12	0.020
C2T1	16.1	11.7	8.0	668	1.04	0.070
C0T3	10.8	4.8	8.5	831	0.71	0.076
C1T3	10.0	4.7	7.5	641	0.61	0.077
C2T3	18.0	11.4	10.7	749	0.83	0.13

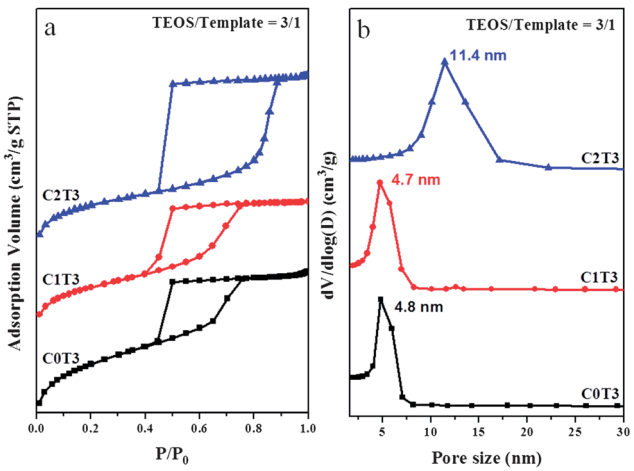

Fig. 12 (a) Nitrogen adsorption/desorption isotherms and (b) pore size distribution curves of mesoporous silicas templated by F127, CFC1, and CFC2 at TEOS-to-template weight ratios of 3 : 1.

silica materials. In this case, much like that observed at a TEOS-to-template ratio of 1 : 1, the *d*-spacing decreased initially when we increased the molecular weight of the PCL segments, but it increased thereafter. Scheme 1 summarizes the detailed morphological changes that occurred to the mesoporous silica samples upon increasing the molecular weight of the PCL segments at TEOS-to-template ratios of 1 : 1 and 3 : 1.

Conclusions

We have used an EISA strategy to synthesize long-range-ordered mesoporous silicas, templated by F127; the morphologies of the mesostructures could be controlled from hexagonal cylinder structures to bcc structures merely by changing the amounts of added TEOS. In addition, we also examined the effects of PCL segments in ABCBA-type multiblock copolymers of PCL-F127-PCL on the morphologies of the mesoporous silica samples. We found that the *d*-spacings and average pore sizes both decreased initially, but increased thereafter, upon increasing the molecular weight of the PCL segments in the template. Because of their large surface areas, pore sizes, and pore volumes, the resulting long-range-ordered mesoporous silicas might have potential applications within chemical sensors or fuel cells. Using this approach, we can prepare highly ordered mesoporous silicas having narrow pore size distributions and various morphologies when applying ABA-type triblock and ABCBA-type multiblock copolymers as templates.

Acknowledgements

This study was supported financially by the National Science Council, Taiwan, Republic of China, under contracts NSC 100-2221-E-110-029-MY3 and NSC 100-2628-E-110-001.

Notes and references

1 A. Corma, *Chem. Rev.*, 1997, **97**, 2373.
2 K. Ariga, A. Vinu, O. Ji, O. OOhmori, J. P. Hill, S. Acharya, J. Koike and S. Shiratori, *Angew. Chem., Int. Ed.*, 2008, **120**, 7364.
3 M. Vallet-Regi, F. Balas and D. Acros, *Angew. Chem., Int. Ed.*, 2007, **46**, 7548.
4 K. Ariga, A. Vinu, T. Yamauchi, Q. Ji and J. P. Hill, *Bull. Chem. Soc. Jpn.*, 2012, **1**, 1.
5 P. Yang, D. Zhao, D. I. Margolese, B. F. Chmelka and G. D. Stucky, *Chem. Mater.*, 1999, **11**, 2813.
6 J. S. Beck, J. C. Vartuli, W. J. Roth, M. E. Leonowicz, C. T. Kresge, K. D. Schmitt, C. T. W. Chu, D. H. Olson, E. W. Sheppard, S. B. McCullen, J. B. Higgins and J. L. Schlenker, *J. Am. Chem. Soc.*, 1992, **114**, 10834.
7 C. T. Kresge, M. E. Leonowicz, W. J. Roth, J. C. Vartuli and J. S. Beck, *Nature*, 1992, **359**, 710.
8 D. Y. Zhao, J. L. Feng, Q. S. Huo, N. Melosh, G. H. Fredrickson, B. F. Chmelka and G. D. Stucky, *Science*, 1998, **279**, 548.
9 D. Y. Zhao, Q. S. Huo, J. L. Feng, B. F. Chmelka and G. D. Stucky, *J. Am. Chem. Soc.*, 1998, **120**, 6024.
10 J. G. Li and S. W. Kuo, *RSC Adv.*, 2011, **1**, 1822.
11 Y. H. Deng, T. Yu, Y. Wan, Y. F. Shi, Y. Meng, D. Gu, L. J. Zhang, Y. Huang, C. Liu, X. J. Wu and D. Y. Zhao, *J. Am. Chem. Soc.*, 2007, **129**, 1690.
12 M. Mandal and M. Kruk, *Chem. Mater.*, 2012, **24**, 149.
13 Y. F. Lee, K. H. Chang, C. Y. Chu, H. L. Chen and C. C. Hu, *RSC Adv.*, 2011, **1**, 401.
14 J. G. Li, R. B. Lin and S. W. Kuo, *Macromol. Rapid Commun.*, 2012, **33**, 678.
15 S. P. Naik, W. Fan, T. Yokoi and T. Okubo, *Langmuir*, 2006, **22**, 6391.
16 K. Yu, A. J. Hurd, A. Eisenberg and C. J. Brinker, *Langmuir*, 2001, **17**, 7961.
17 C. Liu, Y. H. Deng, J. Liu, H. H. Wu and D. Y. Zhao, *Microporous Mesoporous Mater.*, 2008, **116**, 633.
18 Z. D. Zhang, X. X. Yan, B. Z. Tian, C. Z. Yu, B. Tu, G. S. Zhu, S. L. Qiu and D. Y. Zhao, *Microporous Mesoporous Mater.*, 2006, **90**, 23.
19 M. Mandal and M. Kruk, *Chem. Mater.*, 2012, **24**, 123.
20 A. F. Zhang, K. K. Hou, L. Gu, C. Y. Dai, M. Liu, C. S. Song and X. W. Guo, *Chem. Mater.*, 2012, **24**, 1005.
21 A. P. Katsoulidis and M. G. Kanatzidis, *Chem. Mater.*, 2012, **24**, 471.
22 S. Valkama, A. Nykanen, H. Kosonen, R. Ramani, F. Tuomisto, P. Engelhardt, G. ten Brinke, O. Ikkala and J. Ruokolainen, *Adv. Funct. Mater.*, 2007, **17**, 183.
23 Y. Wan, Y. F. Shi and D. Y. Zhao, *Chem. Commun.*, 2007, 897.
24 J. G. Li, Y. D. Lin and S. W. Kuo, *Macromolecules*, 2011, **44**, 9295.
25 Y. Meng, D. Gu, F. Q. Zhang, Y. F. Shi, L. Cheng, D. Feng, Z. X. Wu, Z. X. Chen, Y. Wan, A. Stein and D. Y. Zhao, *Chem. Mater.*, 2006, **18**, 4447.
26 Y. Wan, Y. F. Shi and D. Y. Zhao, *Chem. Mater.*, 2008, **20**, 932.
27 Y. Meng, D. Gu, F. Q. Zhang, Y. F. Shi, H. F. Yang, Z. Li, C. Z. Yu, B. Tu and D. Y. Zhao, *Angew. Chem., Int. Ed.*, 2005, **44**, 7053.
28 W. C. Chu, J. G. Li and S. W. Kuo, *RSC Adv.*, 2013, **3**, 6485.
29 L. Y. Song, D. Feng, N. J. Fredin, K. G. Yager, R. L. Jones, Q. Y. Wu, D. Y. Zhao and B. D. Vogt, *ACS Nano*, 2010, **4**, 189.
30 H. Wei, Y. Y. Lv, L. Han, B. Tu and D. Y. Zhao, *Chem. Mater.*, 2011, **23**, 2353.
31 J. Y. Zhang, Y. H. Deng, J. Wei, Z. K. Sun, D. Gu, H. Bongard, C. Liu, H. H. Wu, B. Tu, F. Schuth and D. Y. Zhao, *Chem. Mater.*, 2009, **21**, 3996.
32 Y. H. Deng, J. Liu, C. Liu, D. Gu, Z. K. Sun, J. Wei, J. Y. Zhang, L. J. Zhang, B. Tu and D. Y. Zhao, *Chem. Mater.*, 2008, **20**, 7281.
33 Y. Deng, C. Liu, D. Gu, T. Yu, B. Tu and D. Zhao, *J. Mater. Chem.*, 2008, **18**, 91.
34 L. Sterk, J. Gorka, A. Vinu and M. Jaroniec, *Microporous Mesoporous Mater.*, 2012, **156**, 121.
35 Y. Huang, J. P. Yang, H. Q. Cai, Y. P. Zhai, D. Feng, Y. H. Deng, B. Tu and D. Y. Zhao, *J. Mater. Chem.*, 2009, **19**, 6536.
36 E. Nisson, Y. Sakamoto and A. E. C. Palmqvist, *Chem. Mater.*, 2011, **23**, 2781.

37 D. Grosso, C. Boissiere, B. Smarsly, T. Brezesinski, N. Pinna, P. A. Albouy, H. Amenitsch, M. Antonietti and C. Sanchez, *Nat. Mater.*, 2004, **3**, 787.
38 E. Ortel, A. Fischer, L. Chuenchom, J. Polte, F. Emmerling, B. Smarsly and R. Kraehnert, *Small*, 2012, **8**, 298.
39 K. Kailasam, Y. S. Jun, P. Katekomol, J. D. Epping, W. H. Hong and A. Thomas, *Chem. Mater.*, 2010, **22**, 428.
40 R. L. Liu, Y. F. Shi, Y. Wan, Y. Meng, F. Q. Zhang, D. Gu, Z. X. Chen, B. Tu and D. Y. Zhao, *J. Am. Chem. Soc.*, 2006, **128**, 11652.
41 D. Y. Zhao, Q. S. Huo, J. L. Feng, B. F. Chmelka and G. D. Stucky, *J. Am. Chem. Soc.*, 1998, **120**, 6024.
42 X. Y. Bao, X. S. Zhao, X. Li, P. A. Chia and J. Li, *J. Phys. Chem. B*, 2004, **108**, 4684.
43 L. Cao and M. Kruk, *Colloids Surf., A*, 2010, **357**, 91.
44 J. P. Hanrahan, A. Donovan, M. A. Morris and J. D. Holmes, *J. Mater. Chem.*, 2007, **17**, 3881.
45 S. S. Kim, A. Karkamkar, T. J. Pinnavaia, M. Kruk and M. Jaroniec, *J. Phys. Chem. B*, 2001, **105**, 7663.
46 T. W. Kim, F. Kleitz, B. Paul and R. Ryoo, *J. Am. Chem. Soc.*, 2005, **127**, 7601.
47 B. Z. Tian, X. Y. Liu, Z. D. Zhang, B. Tu and D. Y. Zhao, *J. Solid State Chem.*, 2002, **167**, 324.
48 D. H. Chen, Z. W. Li, Y. X. J. Tu, Y. F. Shi, Z. X. Chen, W. Shen, C. Z. Yu, B. Tu and D. Y. Zhao, *J. Mater. Chem.*, 2006, **16**, 1511.
49 J. Lee, J. Kim, Y. Lee, S. Yoon, S. M. Oh and T. Hyeon, *Chem. Mater.*, 2004, **16**, 3323.
50 Z. Y. Wang and A. Stein, *Chem. Mater.*, 2008, **20**, 1029.
51 F. Q. Zhang, Y. Meng, D. Gu, Y. Yan, Z. X. Chen, B. Tu and D. Y. Zhao, *Chem. Mater.*, 2006, **18**, 5279.
52 Y. Song, D. Feng, C. G. Campbell, D. Gu, A. M. Forster, K. G. Yager, N. Fredin, H. J. Lee, R. L. Jones, D. Y. Zhao and B. D. Vogt, *J. Mater. Chem.*, 2010, **20**, 1691.
53 C. Urata, Y. Tamura, Y. Yamauchi and K. Kuroda, *J. Mater. Chem.*, 2011, **21**, 3711.
54 G. W. Zhou, Y. J. Chen, J. H. Yang and S. H. Yang, *J. Mater. Chem.*, 2007, **17**, 2839.
55 H. P. Lin, C. Y. Chang-Chien, C. Y. Tang and C. Y. Lin, *Microporous Mesoporous Mater.*, 2006, **93**, 344.
56 M. H. Sorensen, R. W. Corkery, J. S. Pedersen, J. Rosenholm and P. C. Alberius, *Microporous Mesoporous Mater.*, 2008, **113**, 1.
57 L. M. Wang, B. Z. Tian, J. Fan, X. Y. Liu, H. F. Yang, C. Z. Yu, B. Tu and D. Y. Zhao, *Microporous Mesoporous Mater.*, 2004, **67**, 123.
58 J. F. Yao, H. T. Wang, K. Y. Chan, L. X. Zhang and N. P. Xu, *Microporous Mesoporous Mater.*, 2005, **82**, 183.
59 J. G. Li, Y. H. Chang, Y. S. Lin and S. W. Kuo, *RSC Adv.*, 2012, **2**, 12973.
60 A. Taguchi and F. Schuth, *Microporous Mesoporous Mater.*, 2005, **77**, 1.
61 J. G. Li, T. S. Lee, K. U. Jeong, C. H. Lin and S. W. Kuo, *RSC Adv.*, 2012, **2**, 11242.
62 M. C. Chao, C. H. Chang, H. P. Lin, C. Y. Tang and C. Y. Lin, *J. Mater. Sci.*, 2009, **44**, 6453.
63 L. Chen, Y. M. Wang and M. Y. He, *J. Porous Mater.*, 2011, **18**, 211.
64 Q. R. Chen, Y. Sakamoto, O. Terasaki and S. A. Che, *Microporous Mesoporous Mater.*, 2007, **105**, 24.
65 J. Hu, J. J. Wang, L. H. Zhou, S. H. Xie and H. L. Liu, *Acta Phys.-Chim. Sin.*, 2006, **22**, 679.
66 Y. K. Hwang, K. R. Patil, S. H. Jhung, J. S. Chang, Y. J. Ko and S. E. Park, *Microporous Mesoporous Mater.*, 2005, **78**, 245.
67 S. K. Jana, R. Nishida, K. Shindo, T. Kugita and S. Namba, *Microporous Mesoporous Mater.*, 2004, **68**, 133.
68 Q. Xiao, Y. J. Zhong, W. D. Zhu, T. H. Chen and L. Wang, *Microporous Mesoporous Mater.*, 2008, **116**, 339.
69 C. Z. Yu, J. Fan, B. Z. Tian and D. Y. Zhao, *Chem. Mater.*, 2004, **16**, 889.
70 C. Y. Chiu, W. H. Hsu, Y. J. Yen, S. W. Kuo and F. C. Chang, *Macromolecules*, 2005, **38**, 6640.
71 Y. K. Jung, M. H. Park, H. J. Moon, U. P. Shinde and B. Jeong, *Macromolecules*, 2013, **46**, 4215.
72 Y. H. Deng, T. Yu, Y. Wan, Y. F. Shi, Y. Meng, D. Gu, L. J. Zhang, Y. Huang, C. Liu, X. J. Wu and D. Y. Zhao, *J. Am. Chem. Soc.*, 2007, **129**, 1690.